IIETA International Information and Engineering Technology Association
Advancing the World of Information and Engineering

Annales de Chimie - Science des Matériaux
Vol. 50, No. 2, April, 2026, pp. 187-195
Journal homepage: http://iieta.org/journals/acsm

Microstructural Characteristics and Compressive Strength of Fly Ash and Marine Bio-Calcium Ternary Cement Paste

Chakkarphan Sangsuwan[1], Worachai Ponloa[2*]

[1] Civil Engineering Department, Rajamangala University of Technology Phra Nakhon, Bangkok 10800, Thailand
[2] Civil Engineering Department, Bangkokthonburi University, Bangkok 10170, Thailand

Corresponding Author Email: worachai.p@ku.th

https://doi.org/10.18280/acsm.500210

Received: 15 January 2026
Revised: 2 April 2026
Accepted: 8 April 2026
Available online: 30 April 2026

Keywords:
fly ash, marine bio-calcium, ternary cement paste, microstructure, Ca–Si composition

ABSTRACT

Supplementary materials improve sustainability and reduce cement consumption in modern cementitious systems. This study investigates the interaction between fly ash (FA) and marine bio-calcium (cuttlebone powder, CBP) in ternary cement paste at different water-to-binder ratios. Ordinary Portland cement (OPC), FA, and CBP were used at a ratio of 80:10:10 by weight with water-to-binder ratios of 0.4, 0.5, 0.6, and 0.7. Compressive strength, scanning electron microscopy–energy-dispersive spectroscopy (SEM–EDS), and thermogravimetric analysis (TGA) were used to evaluate mechanical, microstructural, and thermal behavior. Compressive strength decreases with increasing w/b in both systems. The control decreases from 57.4 to 28.8 MPa, and the ternary system decreases from 51.7 to 27.2 MPa. The ternary mixtures show slightly lower strength than the control mixtures, with differences of 5–10%. EDS analysis shows that the Ca/Si ratio reflects local compositional variations. TGA results indicate lower CH mass loss in the ternary mixtures, with reductions of 6–38% compared with the control. The ternary paste shows comparable microstructural characteristics across all w/b ratios. The results indicate that CBP can be used in ternary cement systems, with a slight reduction in compressive strength.

1. INTRODUCTION

Ordinary Portland cement (OPC) is the primary binder used in modern construction due to its reliable mechanical performance and well-established production technology [1]. However, OPC production requires high energy consumption and generates significant carbon dioxide emissions, which contribute to global environmental concerns [2, 3]. To reduce clinker consumption and mitigate environmental impacts, many studies have investigated the incorporation of supplementary cementitious materials (SCMs) in cement-based systems [4, 5]. The use of SCMs has therefore become an effective strategy for improving the sustainability of cementitious materials while maintaining adequate engineering performance [6].

Fly ash (FA) is one of the most widely used SCMs in cement-based systems due to its pozzolanic reactivity and its potential to improve long-term mechanical performance [7, 8]. FA reacts with calcium hydroxide produced during cement hydration and forms additional calcium silicate hydrate (C–S–H), which contributes to microstructural densification and improved durability of cementitious materials [9]. In addition, the incorporation of FA reduces clinker consumption in cement-based systems and therefore lowers energy demand and carbon emissions associated with cement production [10].

In recent years, ternary cementitious systems incorporating multiple mineral additives have attracted increasing research attention because they offer potential benefits in both engineering performance and environmental sustainability [7-9]. By combining different supplementary materials, ternary systems modify the hydration process and influence the formation of hydration products and the evolution of microstructure in cement-based materials [10-12]. The interaction among mineral components influences calcium ion availability, the development of hydration phases, and the structural characteristics of the cement matrix [11, 12]. Consequently, ternary binder systems provide an effective approach for improving material performance while simultaneously enhancing the sustainability of cementitious materials [7, 10].

Calcium carbonate occurs in several polymorphic forms, including calcite and aragonite [13, 14]. Aragonite attracts research interest because it can act as a precursor mineral in phase transformation processes [15, 16]. Marine bio-calcium materials derived from natural marine sources mainly contain aragonite, and researchers investigate them as alternative mineral additives in cement-based materials [17-20]. Marine-derived biomaterials such as cuttlebone also represent sustainable mineral resources because they originate from marine waste and contain $CaCO_3$-rich aragonite structures [21]. Aragonite-rich marine bio-calcium can influence hydration behavior and hydration product formation because it supplies additional calcium to the cementitious system [15, 17].

Despite the increasing interest in ternary cementitious systems and calcium-based additives, the interaction between FA and aragonite-based marine bio-calcium in ternary cement paste remains insufficiently understood [22-24]. In particular, limited information is available on how the combined incorporation of these materials influences microstructural characteristics, Ca–Si elemental environment, and phase-related thermal behavior in ternary cement paste [25-28]. Understanding this interaction is important because it governs the pozzolanic reaction, leading to C–S–H formation, microstructural densification, and improved mechanical and durability performance of cementitious materials [29, 30].

Therefore, this study investigates the interaction behavior and microstructural evolution of a FA– marine bio-calcium (cuttlebone powder, CBP) ternary cement paste at different water-to-binder ratios. Mechanical performance, microstructure, Ca–Si compositional characteristics, and phase-related thermal behavior are examined using compressive strength testing, scanning electron microscopy (SEM), energy-dispersive spectroscopy (EDS), and thermogravimetric analysis (TGA).

2. MATERIALS AND METHODS

2.1 Materials

OPC conforming to ASTM C150/C150M-24 [31] served as the primary binder. Class F FA meeting ASTM C618-25a [32] was used as a supplementary cementitious material. These materials formed the base of the ternary binder system. Marine bio-calcium powder (cuttlebone powder, CBP) was derived from cuttlebone waste generated by the seafood processing industry. The material was dried and ground prior to use. The powder passed through a No. 100 sieve (150 μm). Sieve analysis followed ASTM C136/C136M-25 [33] to control particle size distribution.

All constituents were used in dry powder form. The binder system consisted of OPC, Class F FA, and marine bio-calcium in controlled proportions. This system enabled the evaluation of phase interaction and microstructural development in the ternary cement paste.

Table 1. Chemical composition of Ordinary Portland cement (OPC), fly ash (FA), and cuttlebone powder (CBP) determined by X-ray fluorescence (XRF) (% by weight).

Element (wt%)	OPC	FA	CBP
Al	2.38	11.58	0.02
Ca	58.38	1.50	69.07
Cl	0.06	-	0.27
Fe	3.36	3.83	0.09
K	0.43	0.96	0.10
Mg	0.63	0.16	0.04
Mn	0.08	0.04	-
Na	0.16	0.26	0.43
O	23.87	35.68	29.43
P	0.03	0.06	0.08
S	0.68	0.06	0.09
Si	9.67	44.76	0.06
Sr	0.02	0.06	0.33
Ti	0.24	0.90	-
Zr	-	0.09	-

The chemical compositions of OPC, FA, and CBP were determined by X-ray fluorescence (XRF), as presented in Table 1. OPC contains mainly calcium-based phases. FA is rich in silica and alumina. CBP has a high calcium content. These compositions define the role of each material in the ternary binder system. OPC acts as the primary binder. FA serves as a silica–alumina-rich supplementary material, and CBP provides a calcium-rich component.

2.2 Mix proportion

The mixtures were divided into two groups. The first group consisted of plain cement paste without any mineral addition, and this group served as the control system. The second group consisted of ternary cement paste incorporating FA and marine bio-calcium as partial replacement of OPC by mass of binder. Four water-to-binder (w/b) ratios were investigated, including 0.4, 0.5, 0.6, and 0.7. All mixture proportions are summarized in Table 2.

Table 2. Specimen mixture proportions

Specimen ID	OPC (wt.%)	CBP (wt.%)	FA (wt.%)	w/b Ratio
C4	100	0	0	0.4
C5	100	0	0	0.5
C6	100	0	0	0.6
C7	100	0	0	0.7
OCF4	80	10	10	0.4
OCF5	80	10	10	0.5
OCF6	80	10	10	0.6
OCF7	80	10	10	0.7

Note: OPC = Ordinary Portland cement; CBP = cuttlebone powder; FA = fly ash.

2.3 Specimen preparation and curing

Cement paste mixtures were prepared using a mechanical mixer in accordance with ASTM C305-20 [34]. The dry binder components were blended before water addition. Water was introduced according to the designated water-to-binder ratio, and mixing continued until a uniform paste was obtained. The fresh paste was cast into 50 × 50 × 50 mm cube molds following ASTM C109/C109M-20 [35]. The specimens remained in the molds for 24 h. After demolding, all cubes were cured in water in accordance with ASTM C511-21 [36] at 22 ± 2 ℃ for 28 days. At the end of the curing period, three cube specimens from each group were tested for compressive strength. The remaining specimens were prepared for microstructural examination using SEM and EDS.

2.4 Compressive strength test

Compressive strength was determined in accordance with ASTM C109/C109M-20 [35] at 28 days using 50 × 50 × 50 mm cube specimens. Load was applied continuously to failure using a calibrated compression testing machine conforming to ASTM E4-20 [37]. The maximum failure load was recorded for each specimen. Compressive strength was calculated by dividing the failure load by the loaded area. Three specimens were tested for each mixture. The mean value and standard deviation (SD) were reported.

2.5 Microstructural analysis (scanning electron microscopy and energy-dispersive spectroscopy)

Microstructural features were examined using SEM. Fractured surfaces obtained after compressive testing were

used for analysis. Samples were dried prior to observation to ensure stable surface conditions. Elemental composition was determined using EDS integrated with the SEM system. Atomic percentages of calcium (Ca) and silicon (Si) were recorded from selected regions. These measurements provided compositional data for the ternary cement paste system.

2.6 Thermal analysis

TGA was performed to evaluate the thermal behavior of hydrated cement paste. Hydration was terminated using acetone prior to sample preparation. The specimens were dried and ground into powder for analysis. The samples were heated from 50 to 1000 ℃ at a constant rate of 10 ℃/min under a nitrogen (N_2) atmosphere. Mass loss was recorded as a function of temperature.

The TGA results were interpreted using mass loss over defined temperature ranges obtained directly from the thermogravimetric curves. The mass loss in the range of 400–450 ℃ was attributed to the decomposition of calcium hydroxide (CH) based on the observed inflection points. The results are presented as raw mass loss without stoichiometric conversion. Possible overlap with carbonate decomposition at higher temperatures (~650–700 ℃) was considered.

3. RESULTS AND DISCUSSION

3.1 Compressive strength behavior

The compressive strength of the control cement paste and the FA–CBP ternary cement paste at different w/b values appears in Figure 1. Compressive strength decreases as the w/b increases in both systems. The control paste exhibits a compressive strength of 57.39 MPa at w/b = 0.4, which decreases to 28.65 MPa at w/b = 0.7. The ternary system exhibits a similar trend. Compressive strength decreases from 51.65 MPa at w/b = 0.4 to 27.15 MPa at w/b = 0.7. At all w/b values, the ternary mixtures exhibit slightly lower compressive strength than the control paste. The strength reduction is 10.02% at w/b = 0.4, 6.36% at w/b = 0.5, 6.23% at w/b = 0.6, and 5.24% at w/b = 0.7.

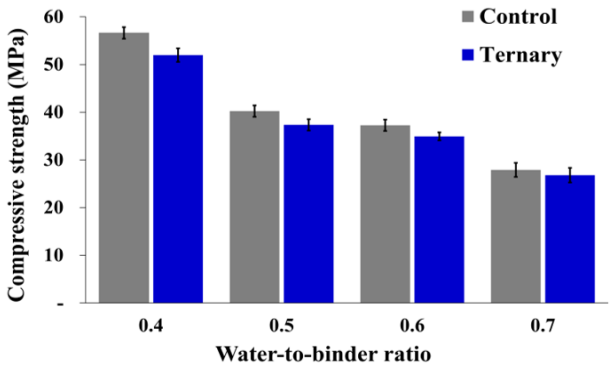

Figure 1. Effect of w/b on compressive strength

The reduction in compressive strength with increasing w/b indicates that the internal structure of the cement paste becomes less compact as the water content increases. A higher w/b increases the spacing between cement particles and reduces the density of the hydration matrix after hardening. This condition weakens the load-bearing framework of the hardened paste.

The slightly lower compressive strength observed in the ternary mixtures indicates that the incorporation of FA and CBP modifies the binder composition of the cement paste. The partial replacement of cement reduces the fraction of the primary cement phases that contribute to strength development in the hardened matrix. Consequently, the ternary binder forms a hydration structure that differs from that of the control cement paste.

These mechanical results indicate that both w/b and binder composition influence the development of the internal structure of the hydrated matrix. The microstructural characteristics responsible for this behavior are examined further through SEM observations in the following section.

3.2 Microstructural evolution

SEM micrographs show clear variations in hydration morphology with w/b (Figure 2). At w/b = 0.4, the control paste (Figure 2(a)) exhibits a dense and continuous hydration matrix with limited visible pores. Hydration products form an interconnected framework that fills the inter-particle spaces. The ternary paste at the same ratio (Figure 2(d)) also forms a compact structure, although local heterogeneity appears in some regions. As the w/b increases to 0.6 and 0.7 (Figure 2(b), (c), (e), (f)), the matrix becomes less compact and more irregular. Larger inter-particle spacing and visible pores appear within the hydration structure. The ternary system maintains partial matrix continuity at intermediate w/b, but pore presence becomes more evident at higher water content.

Overall, the control paste exhibits a compact hydration framework at low w/b, while matrix continuity decreases as the w/b increases. The ternary paste follows a similar trend. These microstructural observations provide the structural basis for interpreting elemental distribution in the following section.

3.3 Ca–Si compositional variation (energy-dispersive spectroscopy)

EDS results reveal variations in Ca and Si compositions in the analyzed areas of the control and ternary cement pastes. The relationship between Ca and Si atomic percentages obtained from EDS area analysis appears in Figures 3 and 4. The analyzed areas exhibit different Ca and Si contents among the samples. In the control paste, Ca contents vary between 75.00 and 77.81 at%, while Si contents vary between 21.19 and 25.00 at% for w/b = 0.5–0.7. In the ternary paste containing FA and CBP, Ca contents vary between 76.60 and 80.29 at%, and Si contents vary between 19.71 and 23.40 at% within the same w/b range. The calculated Ca/Si ratios appear in Table 3. The control paste exhibits Ca/Si ratios of 3.00, 3.67, and 3.45 at w/b = 0.5, 0.6, and 0.7, respectively. The ternary paste exhibits Ca/Si ratios of 3.27, 3.41, and 3.70 at the same w/b levels.

Table 3. Ca–Si composition

Sample	w/b	Ca (at %)	Si (at %)	Ca/Si
C4	0.4	88.98	11.02	8.07
C5	0.5	75.00	25.00	3.00
C6	0.6	77.81	21.19	3.67
C7	0.7	77.53	22.47	3.45
OCF4	0.4	80.29	19.71	4.07
OCF5	0.5	76.60	23.40	3.27
OCF6	0.6	77.82	22.82	3.41
OCF7	0.7	78.72	21.28	3.70

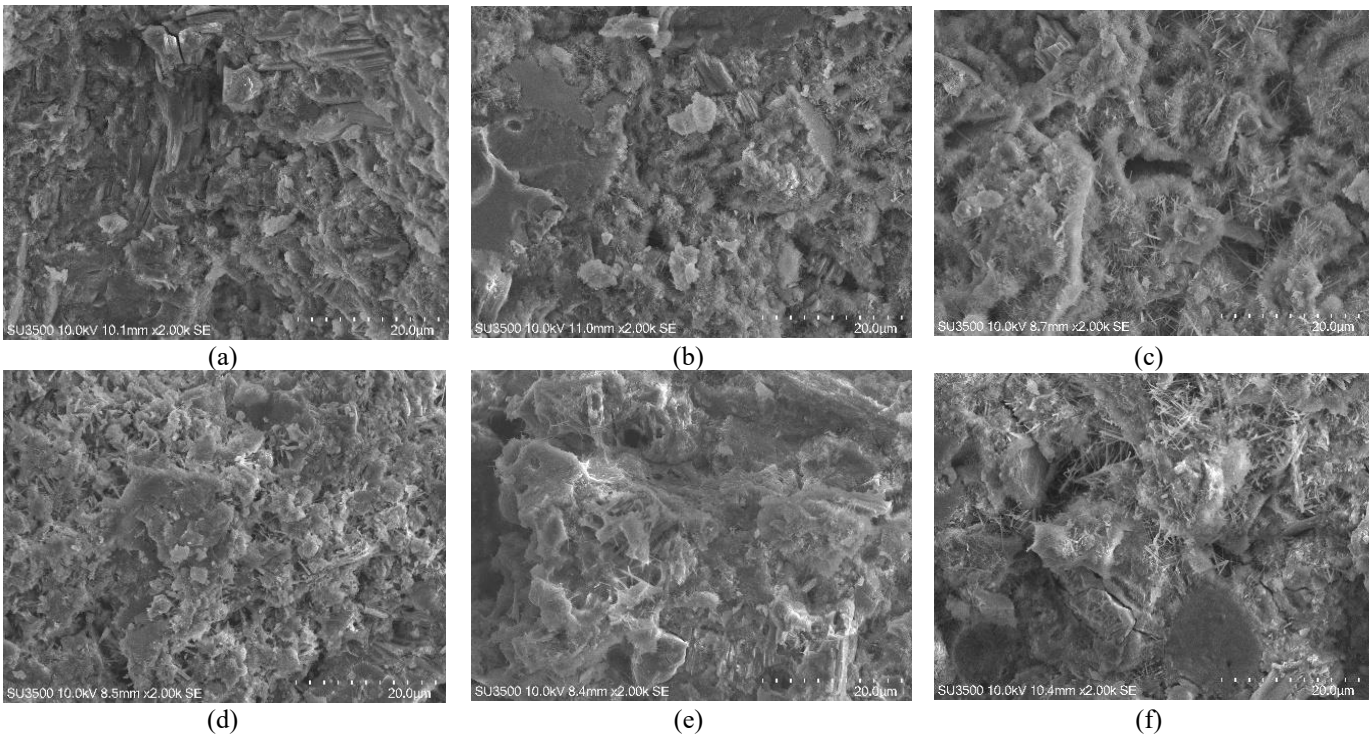

Figure 2. Scanning electron microscopy (SEM) micrographs (2000×) of cement paste microstructures at different water-to-binder ratios at 28 days: (a) C4, (b) C6, (c) C7, (d) OCF4, (e) OCF6, and (f) OCF7

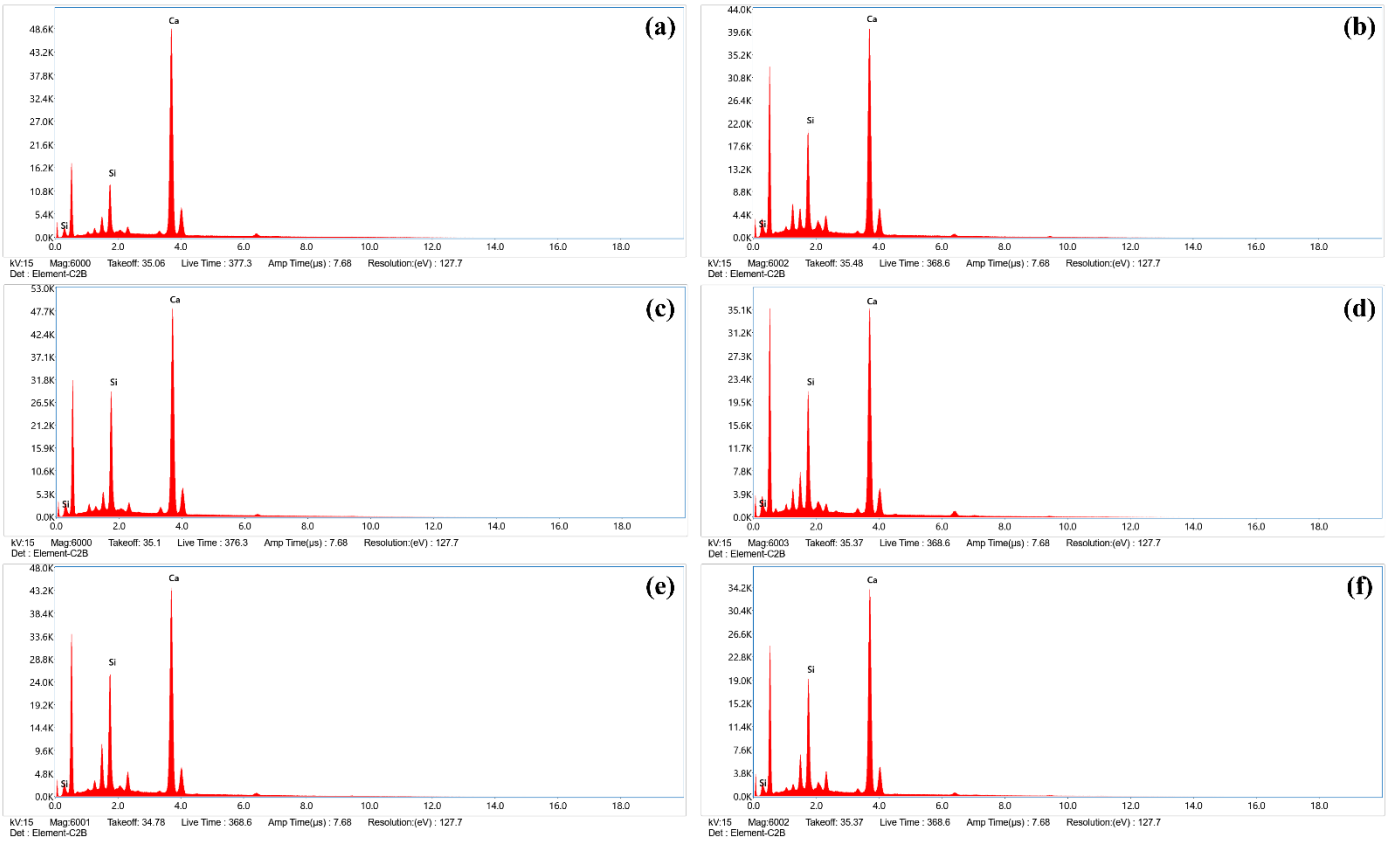

Figure 3. Energy-dispersive spectroscopy (EDS) spectra of control (C) and ternary fly ash–marine bio-calcium cement pastes at different w/b: (a) C4, (b) OCF4, (c) C6, (d) OCF6, (e) C7, and (f) OCF7

The variation of Ca/Si ratios with w/b appears in Figure 5. The measured Ca/Si ratios vary within a comparable range for both paste systems across the investigated w/b values. EDS elemental maps further reveal that Ca and Si are distributed differently within the hydration matrix, as illustrated in Figure 6. Regions with higher Ca intensity correspond to Ca-rich areas, while Si appears more continuously distributed throughout the matrix. This distribution pattern reflects the coexistence of Ca-rich hydration regions and Si-rich matrix phases observed in the SEM micrographs.

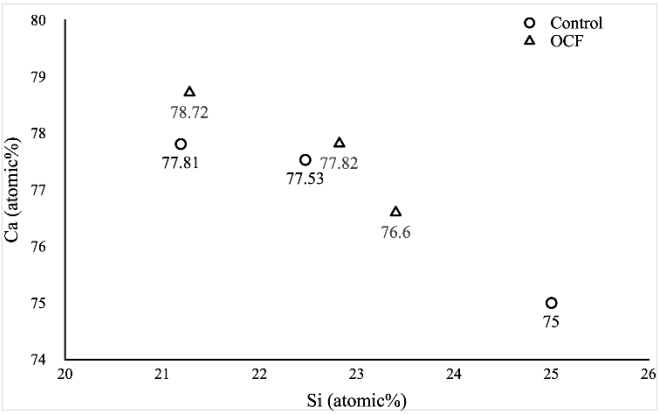

Figure 4. Relationship between Ca and Si atomic percentages derived from energy-dispersive spectroscopy (EDS) area analysis of control (C) and OCF cement pastes at different w/b ratios

The Ca–Si scatter plot further illustrates variations in elemental compositions among the analyzed areas. Areas with higher Si contents tend to exhibit lower Ca contents, indicating differences in the local elemental environment of the hydration products. Taken together, the EDS results provide insight into the elemental characteristics of the hydration matrix in both paste systems. These compositional features provide the chemical context for interpreting the phase-related thermal behavior discussed in the following section.

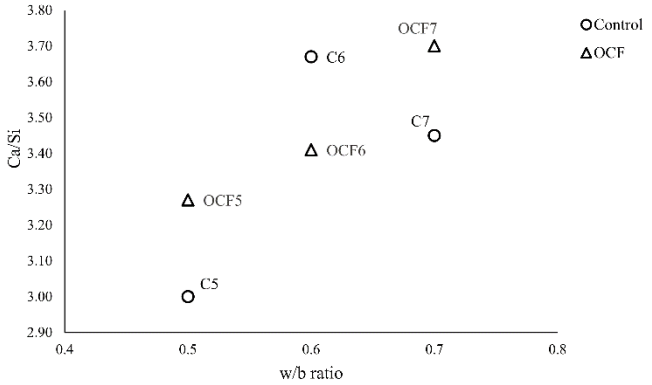

Figure 5. Variation of Ca/Si ratios in control and OCF cement pastes at different w/b ratios derived from energy-dispersive spectroscopy (EDS) compositional analysis

The observed Ca–Si compositional variation indicates changes in the chemical environment of the hydrated cement matrix. Elemental composition alone cannot fully explain the development of hydration products. Thermal analysis is therefore used in the following section to evaluate the evolution of hydration phases in the investigated cement paste system.

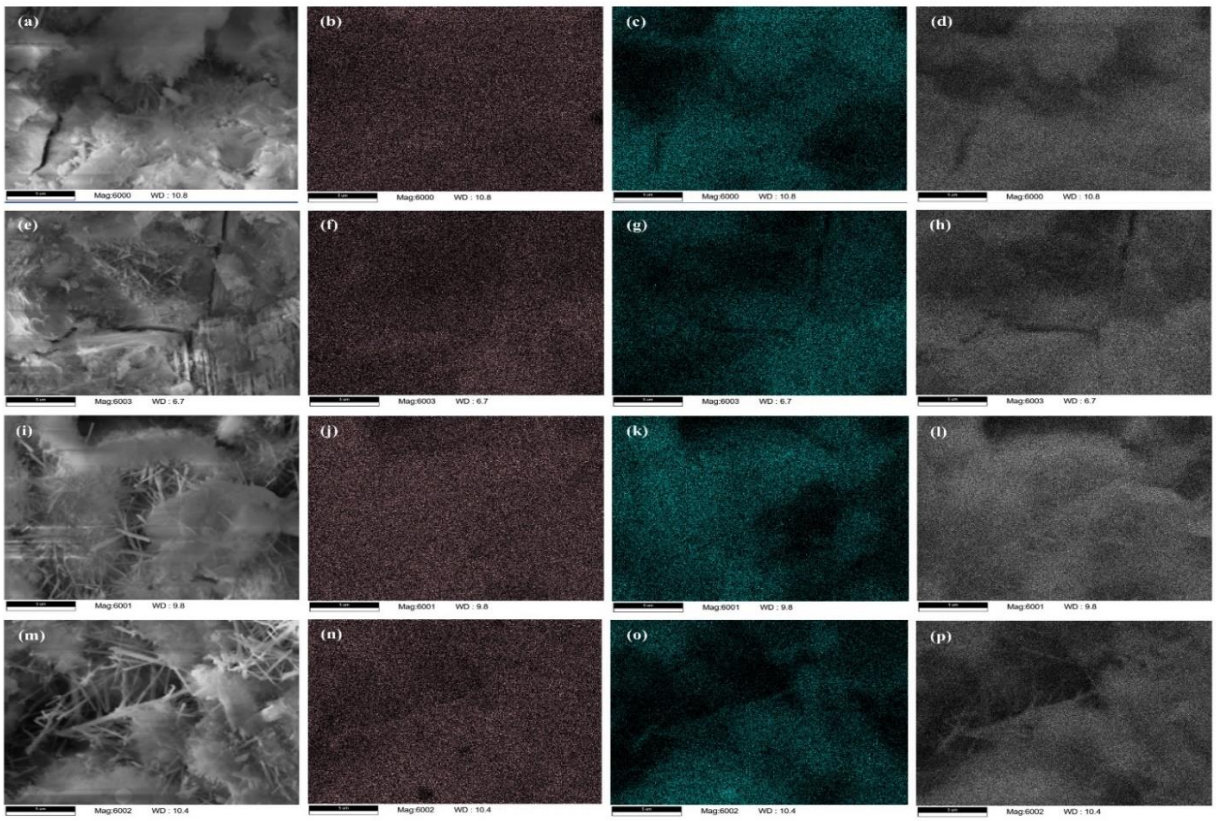

Figure 6. Scanning electron microscopy (SEM) images and corresponding energy-dispersive spectroscopy (EDS) elemental maps showing Ca and Si distributions in control and OCF cement pastes at w/b ratios of 0.5 and 0.7. (a–d) C5, (e–h) OCF5, (i–l) C7, and (m–p) OCF7

3.4 Thermal evidence of phase development

3.4.1 Thermogravimetric analysis results

Mass-loss distributions change as w/b increases from 0.4 to 0.7 in the cement pastes. The summarized TGA results appear in Figure 7. A quantitative comparison of the mass losses corresponding to the identified thermal regions is presented in Figure 8. The thermal decomposition regions and their

corresponding phase interpretations are summarized in Table 4. Bound-water mass loss in the control mixtures decreases from 15.65% to 12.69% as w/b increases. The OCF mixtures remain relatively stable within 11.36–12.80%. Portlandite mass loss in the control mixtures decreases from 7.56% to 6.68%, whereas the OCF mixtures increase from 5.37% to 6.87%.

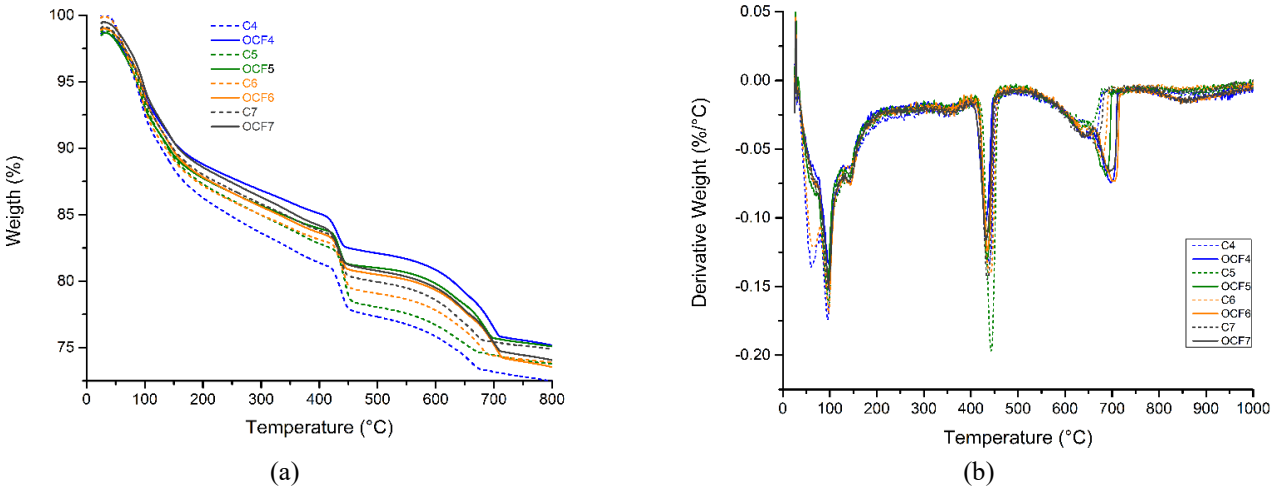

(a) (b)

Figure 7. Thermogravimetric analysis (TGA) of cement pastes incorporating marine bio-calcium. (a) TGA curves showing the mass loss behavior of control and OCF systems. (b) Derivative thermogravimetry (DTG) curves highlighting the thermal decomposition peaks associated with bound water, portlandite, and carbonate phases

Table 4. Thermal decomposition regions and phase interpretation derived from thermogravimetric analysis (TGA)

Temperature Range	Decomposition Process	Phase Interpretation	Significance in This Study
<200 ℃	dehydration	bound water in C–S–H and hydrated phases	indicates hydration degree
400–450 ℃	dehydroxylation	$Ca(OH)_2$ (portlandite)	reflects CH formation during hydration
650–700 ℃	decarbonation	$CaCO_3$ phases	associated with carbonate phases from marine bio-calcium

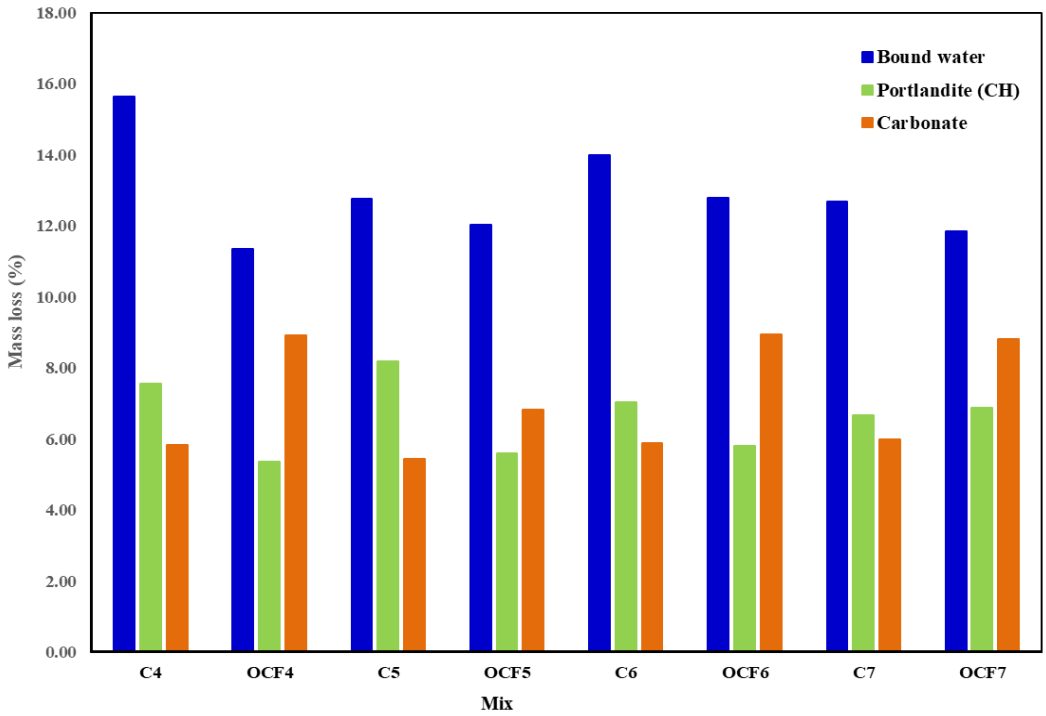

Figure 8. Quantitative comparison of mass loss corresponding to the three thermal regions

Carbonate mass loss in the control mixtures remains nearly constant within 5.45–6.00%. The OCF mixtures show higher carbonate mass loss ranging from 6.82–8.95% across all w/b values. At the same w/b, the control mixtures show higher

mass loss in the bound-water and portlandite regions. Bound-water mass loss exceeds that of the OCF mixtures by 6–38%. Portlandite mass loss is 21–46% higher in the control mixtures. In contrast, carbonate mass loss is 25–53% higher in the OCF mixtures. The defined temperature intervals show consistent behavior across all samples.

3.4.2 Derivative thermogravimetry results

Derivative thermogravimetry (DTG) curves show three main derivative peaks at approximately 80–120 ℃, 420–450 ℃, and 650–720 ℃. These peaks appear in both the control and OCF mixtures at all w/b values. The corresponding DTG curves appear in Figure 7. The peak near 100 ℃ represents the release of bound water from hydrated phases. The control mixtures show deeper peaks in this temperature range than the OCF mixtures. The peak near 430 ℃ represents the dehydroxylation of $Ca(OH)_2$, which corresponds to the decomposition of portlandite (CH). The control mixtures again show deeper peaks in this region. The peak near 680–700 ℃ represents the decomposition of carbonate phases. The OCF mixtures show deeper derivative peaks than the control mixtures in this temperature range.

The thermogravimetric results reflect the thermal behavior of hydration products observed in the previous sections. The bound-water region between 80–120 ℃ corresponds to dehydration of hydrated phases and indicates the hydration degree within the paste matrix. The control mixtures exhibit higher bound-water mass loss than the OCF mixtures. This result suggests a larger amount of hydrated phases in the control paste within this temperature range. The SEM observations in Section 3.2 also show a dense hydration framework in the control paste at lower w/b, which supports this thermal behavior.

The peak near 420–450 ℃ corresponds to the dehydroxylation of $Ca(OH)_2$, which represents the decomposition of portlandite (CH). The deeper DTG peaks in the control mixtures indicate higher CH content compared with the OCF mixtures. The EDS results in Section 3.3 also reveal Ca-rich regions in the hydration matrix, which correspond to these CH-related thermal features. The carbonate decomposition region between 650–720 ℃ shows a different trend. The OCF mixtures exhibit higher carbonate mass loss than the control mixtures. This result indicates a greater presence of carbonate phases in the ternary system.

The combined SEM, EDS, and TGA results indicate that the ternary binder system modifies the distribution of hydration products and related thermal phases in the cement paste. The microstructural observations reveal changes in matrix compactness, while the EDS analysis shows variations in Ca–Si elemental environments. The thermogravimetric results further confirm differences in CH and carbonate-related phases between the control and OCF systems. These findings provide the phase-related basis for interpreting the interaction behavior of the fly ash–CBP ternary system discussed in the following section.

3.5 Interaction behavior in the FA-CBP ternary cement system

SEM, EDS, and TGA results together describe the interaction behavior of the FA–CBP ternary cement system. SEM observations show that matrix compactness decreases as the water-to-binder ratio increases. The hydration matrix becomes less dense at higher w/b values, and pore features appear more frequently in the microstructure. EDS analysis reveals variations in the Ca–Si elemental environment of the hydration matrix. However, the Ca–Si distributions and calculated Ca/Si ratios remain within a comparable range for both paste systems across the investigated w/b values. This result indicates that the ternary paste maintains a Ca–Si chemical environment similar to that of the control paste.

Thermogravimetric results show clear differences in phase-related mass loss between the systems. The control mixtures exhibit higher mass loss in the bound-water and portlandite regions, whereas the ternary mixtures exhibit higher carbonate-related mass loss. These thermal characteristics reflect differences in the distribution of hydration and carbonate-related phases within the cement matrix. Taken together, the SEM, EDS, and TGA observations show that the fly ash–CBP ternary system alters the internal phase distribution of the hydrated cement matrix while maintaining a comparable Ca–Si chemical environment.

4. CONCLUSIONS

The mechanical behavior, microstructure, elemental composition, and thermal characteristics of cement pastes incorporating a fly ash–CBP ternary binder were evaluated. Compressive strength decreases with increasing water-to-binder ratio in both the control and ternary systems. The ternary mixtures show slightly lower strength than the control at all investigated ratios. Higher water content increases particle spacing and reduces matrix compactness, which weakens the load-bearing structure of the hardened paste.

Microstructural observations show that the hydration matrix becomes less dense as the water-to-binder ratio increases. Higher water content increases capillary spacing and promotes pore formation. These structural changes reduce matrix continuity and are consistent with the observed mechanical behavior of the cement paste.

Elemental analysis shows that Ca–Si distributions and Ca/Si ratios vary across the analyzed regions in both paste systems. The ternary binder shows comparable local Ca–Si characteristics within the hydration matrix despite the partial replacement of Portland cement.

TGA shows differences in phase-related mass loss between the systems. The control mixtures show higher mass loss in the bound-water and portlandite regions, while the ternary mixtures show higher carbonate-related mass loss. These results indicate that the incorporation of CBP affects the distribution of hydration-related components and carbonate-related components within the cement matrix.

The combined mechanical, microstructural, compositional, and thermal results indicate that the fly ash–CBP ternary system preserves a comparable local Ca–Si chemical environment. However, the incorporation of CBP modifies the distribution of calcium-containing components and increases pore presence within the matrix. These changes reduce matrix continuity and lead to the observed reduction in mechanical performance.

AUTHOR CONTRIBUTIONS

WP conceived and designed the study. WP and CS conducted the experimental work and analyzed the data. CS prepared the manuscript. WP reviewed and improved the manuscript. All authors read and approved the final version of

the manuscript.

ACKNOWLEDGMENT

The authors acknowledge Rajamangala University of Technology Phra Nakhon, Bangkok, Thailand, for providing support for this research.

REFERENCES

[1] Taylor, H.F. (1997). Cement Chemistry. Thomas Telford.

[2] Benhelal, E., Shamsaei, E., Rashid, M.I. (2021). Challenges against CO2 abatement strategies in cement industry: A review. Journal of Environmental Sciences, 104: 84-101. https://doi.org/10.1016/j.jes.2020.11.020

[3] Damtoft, J.S., Lukasik, J., Herfort, D., Sorrentino, D., Gartner, E.M. (2008). Sustainable development and climate change initiatives. Cement and Concrete Research, 38(2): 115-127. https://doi.org/10.1016/j.cemconres.2007.09.008

[4] Monteiro, P. (2006). Concrete: Microstructure, Properties, and Materials. McGraw-Hill Publishing.

[5] Siddique, R. (2014). Utilization of industrial by-products in concrete. Procedia Engineering, 95: 335-347. https://doi.org/10.1016/j.proeng.2014.12.192

[6] Environment, U.N., Scrivener, K.L., John, V.M., Gartner, E.M. (2018). Eco-efficient cements: Potential economically viable solutions for a low-CO2 cement-based materials industry. Cement and concrete Research, 114: 2-26. https://doi.org/10.1016/j.cemconres.2018.03.015

[7] Majhi, R.K., Shin, S.C., Kim, J.M., Patro, S.K. (2026). Towards sustainable cement: Review of blended binder systems and performance-based specification strategies. Materials Today Sustainability, 34: 101328. https://doi.org/10.1016/j.mtsust.2026.101328

[8] Mohammadi, S., Harmon, M.T., O'Shea, E., Clifford, P.C., Ryan, C. (2026). Review of deterioration mechanisms and durability performance mapping of sustainable SCM concrete in wastewater environments. Journal of Building Engineering, 102: 115565. https://doi.org/10.1016/j.jobe.2026.115565

[9] Wang, L., Lu, X. (2024). A review of the influence of aluminum phases from cement, SCMs and external aluminum phases on the thaumasite sulfate attack in cement-based materials. Journal of Building Engineering, 94: 109966. https://doi.org/10.1016/j.jobe.2024.109966

[10] Moolchandani, K. (2025). Industrial byproducts in concrete: A state-of-the-art review. Next Materials, 8: 100593. https://doi.org/10.1016/j.nxmate.2025.100593

[11] Snellings, R., Mertens, G., Elsen, J. (2012). Supplementary cementitious materials. Reviews in Mineralogy and Geochemistry, 74(1): 211-278. https://doi.org/10.2138/rmg.2012.74.6

[12] Richardson, I.G. (2008). The calcium silicate hydrates. Cement and Concrete Research, 38(2): 137-158. https://doi.org/10.1016/j.cemconres.2007.11.005

[13] Sophia, R., Sakthieswaran, N. (2019). Waste shell powders as valuable bio- filler in gypsum plaster - Efficient waste management technique by effective utilization. Journal of Cleaner 220: 74-86. https://doi.org/10.1016/j.jclepro.2019.02.119

[14] Checa, A.G., Cartwright, J.H.E., Sánchez-Almazo, I., Andrade, J.P., Ruiz-Raya, F. (2015). The cuttlefish Sepia officinalis (Sepiidae, Cephalopoda) constructs cuttlebone from a liquid-crystal precursor. Scientific Reports, 5: 11513. https://doi.org/10.1038/srep11513

[15] Kasioptas, A., Geisler, T., Putnis, C.V., Perdikouri, C., Putnis, A. (2010). Crystal growth of apatite by replacement of an aragonite precursor. Journal of Crystal Growth, 312: 2431-2440. https://doi.org/10.1016/j.jcrysgro.2010.05.014

[16] van de Mortel, H., Delaigue, L., Humphreys, M.P., Middelburg, J.J., Ossebaar, S., Bakker, K., Trabucho Alexandre, J.P., van Leeuwen-Tolboom, A.W.E., Wolthers, M., Sulpis, O. (2024). Laboratory observation of the buffering effect of aragonite dissolution at the seafloor. Journal of Geophysical Research: Biogeosciences, 129(2): e2023JG007581. https://doi.org/10.1029/2023JG007581

[17] Mirzabagheri, S., Derhamjani, G., Maharati, S., Ziaee, Z., Vatankhah, F., Mirzabagheri, D. (2018). Using cuttlebone powder to produce green concrete. Journal of Applied Engineering Sciences, 8(2): 25-28. https://doi.org/10.2478/jaes-2018-0014

[18] Ye, J., Liu, S., Fang, J., Zhang, H., Zhu, J., Guan, X. (2023). Synthesis of aragonite whiskers by co-carbonation of waste magnesia slag and magnesium sulfate: Enhancing microstructure and mechanical properties of Portland cement paste. Buildings, 13(11): 2888. https://doi.org/10.3390/buildings13112888

[19] Piras, S., Salathia, S., Guzzini, A., Zovi, A., Jackson, S., Smirnov, A., Fragassa, C., Santulli, C. (2024). Biomimetic use of food-waste sources of calcium carbonate and phosphate for sustainable materials—A review. Materials 17: 843. https://doi.org/10.3390/ma17040843

[20] Wang, H., Li, X., Xuan, M., Yang, R., Zhang, J., Chang, J. (2024). Marine biomaterials for sustainable bone regeneration. Giant, 19: 100298. https://doi.org/10.1016/j.giant.2024.100298

[21] Zulkarnain, N.A.A., Ramli, A., Abd Kadir, N.H. (2024). Optimization on characterization and physicochemical of non-calcined and calcined nanocrystallite of cuttlefish (Sepia officinalis) bones powder for sustainable green technology applications. Biointerface Research in Applied Chemistry, 14(3): 58. https://doi.org/10.33263/BRIAC143.058

[22] Xavier, C.B., Rahim, A.A. (2023). Optimization and characterization of the ternary blended iron rich natural binder concrete system. Construction and Building Materials, 363: 129838. https://doi.org/10.1016/j.conbuildmat.2022.129838

[23] Hartmann, F.A., Mengel, L.C., Plank, J.P. (2022). Effects of exposure to atmospheric moisture and CO_2 on the performance of a ternary binder system and chemical admixtures in a self-levelling underlayment. Construction and Building Materials, 350: 128911. https://doi.org/10.1016/j.conbuildmat.2022.128911

[24] Hou, C., Zheng, L., Lu, X. (2026). Microorganisms as sustainable designers: Releasing productivity and diversity of microbially induced carbonate precipitation from underlying mechanisms to engineered applications. Sustainable Materials and Technologies, 48: e02000.

https://doi.org/10.1016/j.susmat.2026.e02000
[25] Madadi, A., Wei, J. (2026). New insights into the role of Ca/Si ratio in regulating the formation, phase evolution, atomic structure, and macro-performance of calcium silicate hydrates. Journal of Building Engineering, 119: 115170. https://doi.org/10.1016/j.jobe.2025.115170
[26] Han, F., Li, Y., Zhu, Z., Zhang, Z. (2025). Synergistic utilization of Al-rich and carbonate-rich mineral admixtures toward sustainable low-carbon cementitious materials: A review. Journal of Building Engineering 105: 112523. https://doi.org/10.1016/j.jobe.2025.112523
[27] Cheng, Y., Mu, W. (2026). Hydration characteristics, microstructure, and mortar properties of incineration bottom ash-cement composites. Waste and Biomass Valorization, 1-16. https://doi.org/10.1007/s12649-026-03518-x
[28] Xiong, C., Zhang, X., Jin, Z., Yang, H., Shi, C., Cao, M., Lu, M., Zhao, H. (2026). Synergistic effects of Ca/Si and Si/Al ratios on the hydration mechanisms and performance of solid waste-based cementitious materials. Construction and Building Materials, 518: 145804. https://doi.org/10.1016/j.conbuildmat.2026.145804
[29] Velea, A.M., Cabello Galisteo, F., Atanes-Sánchez, E., Nieto-Márquez, A., Martín de Vidales, M.J. (2025). Sustainable management of municipal solid waste incineration fly ash: A life cycle assessment based review of treatment and valorization pathways. Journal of Materials Advances, 19: 100817. https://doi.org/10.1016/j.hazadv.2025.100817
[30] Torres-Ortega, R., Torres-Sanchez, D., Lopez-Lara, T. (2025). Mechanical properties of hydraulic concretes with partial replacement of Portland cement by pozzolans obtained from agro-industrial residues: A review. Heliyon, 11: e41004. https://doi.org/10.1016/j.heliyon.2024.e41004
[31] ASTM C150/C150M-24. (2024). Standard specification for Portland cement. ASTM International, West Conshohocken, PA, USA. https://doi.org/10.1520/C0150_C0150M-24
[32] ASTM C618-25a. (2025). Standard specification for coal ash and raw or calcined natural pozzolan for use in concrete. ASTM International, West Conshohocken, PA, USA. https://doi.org/10.1520/C0618-25A
[33] ASTM C136/C136M-25. (2025). Standard test method for sieve analysis of fine and coarse aggregates. ASTM International, West Conshohocken, PA, USA. https://doi.org/10.1520/C0136_C0136M-25
[34] ASTM C305-20. (2020). Standard Practice for mechanical mixing of hydraulic cement pastes and mortars of plastic consistency. ASTM International, West Conshohocken, PA, USA. https://doi.org/10.1520/C0305-20
[35] ASTM C109/C109M-20. (2020). Standard test method for compressive strength of hydraulic cement mortars (using 2-in. or [50-mm] cube specimens). ASTM International, West Conshohocken, PA, USA. https://doi.org/10.1520/C0109_C0109M-20
[36] ASTM C511-21. (2021). Standard specification for mixing rooms, moist cabinets, moist rooms, and water storage tanks used in the testing of hydraulic cements and concretes. ASTM International, West Conshohocken, PA, USA. https://doi.org/10.1520/C0511-21
[37] ASTM E4-20. (2020). Standard practices for force verification of testing machines. ASTM International, West Conshohocken, PA, USA. http://doi.org/10.1520/E0004-20